

N.Ito, A.Mizohata · R Okumura<sup>1</sup> and Y Iinuma<sup>1</sup>

Radiation Research Center, Osaka Prefecture University,  
<sup>1</sup>Research Reactor Institute, Kyoto University

Central diameters and concentrations of elements (Na, Al, Cl, K, Ca, Ti, V, Cr, Mn, Fe, Co, Ni, Zn, As, Br, Rb, Mo, Sb, Cs, Ba, La, Ce, Sm, Eu, Hf, W and Th) in the atmospheric aerosols collected at Sakai, Osaka in 2012 have been obtained. We have collected aerosols separated by the 9 diameter ranges (<0.43, 0.43~0.65, 0.65~1.1, 1.1~2.1, 2.1~3.3, 3.3~4.7, 4.7~7.0, 7.0~11, >11 μm) using Andersen sampler on one week periods (P1:Feb.14-21, P2:Apr.03-10, P3:Jun05-12, P4:Aug.07-14, P5:Oct.09-16, P6Dec.11-18: in 2012). To collect the samples completely and reduce an affect of contamination we have put polyethylene sheet (80mmΦ, ~1 mg/cm<sup>2</sup>) on the each stage of the sampler.

The element concentrations were analyzed by neutron activation analysis using Kyoto University Nuclear Reactor on following irradiation conditions ( In Pn1 120sec for Al, Cl, Ca, V, Mn, In Pn2 30min for Co, Ni, Zn, As, Br, Rb, Mo, Sb, Cs, Ba, La, Ce, Sm, Eu, Hf, W, Th). Gamma ray spectrum from each irradiated samples were measured by Ge-Solid state detector and 4096channel multiple pulse height analyzer. The measuring time (2000~20000sec) and starts of measurements are determined by the gamma ray intensity of each sample.

From the concentration results in each particle diameter range we have determined the central diameter (d50) which is a diameter of 50% accumulation concentration summing by the each particle diameter range concentration (Fig.1). From the concentrations in each diameter range we get a scatter graph of d50 and total concentrations of each element on 6 sampling periods (Fig.2).

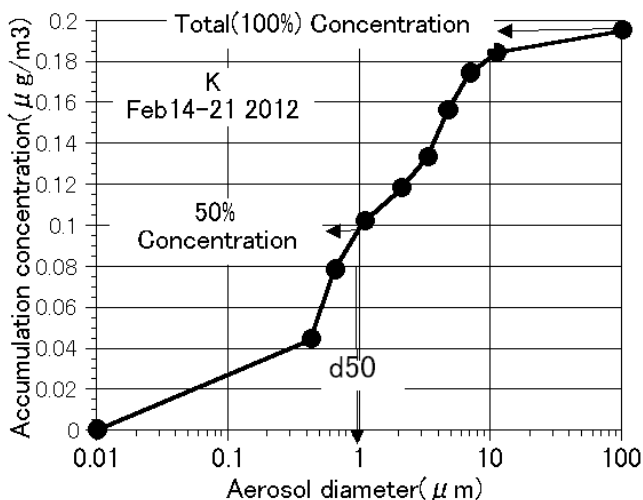


Fig.1 Example of accumulation curve and central diameter (d50) on concentrations of K (Feb14-21 2012) by aerosol diameter in 9 size ranges.

From relations between the d50 and elemental concentrations we have found that Zn, V, Br, Mo, Sb, As have fine d50 (<=2.5 μm) those are Zn (0.9~1.8 μm), V (0.28~0.48 μm), Br (0.34~0.59 μm), Mo (0.24~1.1 μm), Sb (0.957~0.94 μm), As (0.53~1.5 μm).

Al, Na, Fe, Ca, Ti, Ba, Cr, Ce, Co, Th, Hf, Eu have coarse d50 (>=2.5 μm) those are Al (4.6~6.0 μm), Na (3.7~4.3 μm), Fe (3.5~5.1 μm), Ca (4.7~6.2 μm), Ti (4.0~5.9 μm), Ba (2.2~4.1 μm), Cr (2.6~4.9 μm), Ce (3.0~4.7 μm), Co (2.4~4.6 μm), Th (4.0~6.2 μm), Hf (4.5~5.4 μm), Eu (4.4~5.6 μm).

Cl, K, Mo, Ni, W, La, Cs have coarse and fine d50 depending on the sampling period. The variation cause changes of the main constituents in fine d50 depending on the sampling period like that, K, Zn, Mn on P1, Zn on P2, K, Zn on P3, Zn on P4, K, Zn on P5, Cl, K, Zn on P6.

In the fine d50 elements ordered by high to low concentration are Cl, K, Zn, Mn, V, Br, Ni, Mo, Sb, As, W, La of which order changes on the sampling period.

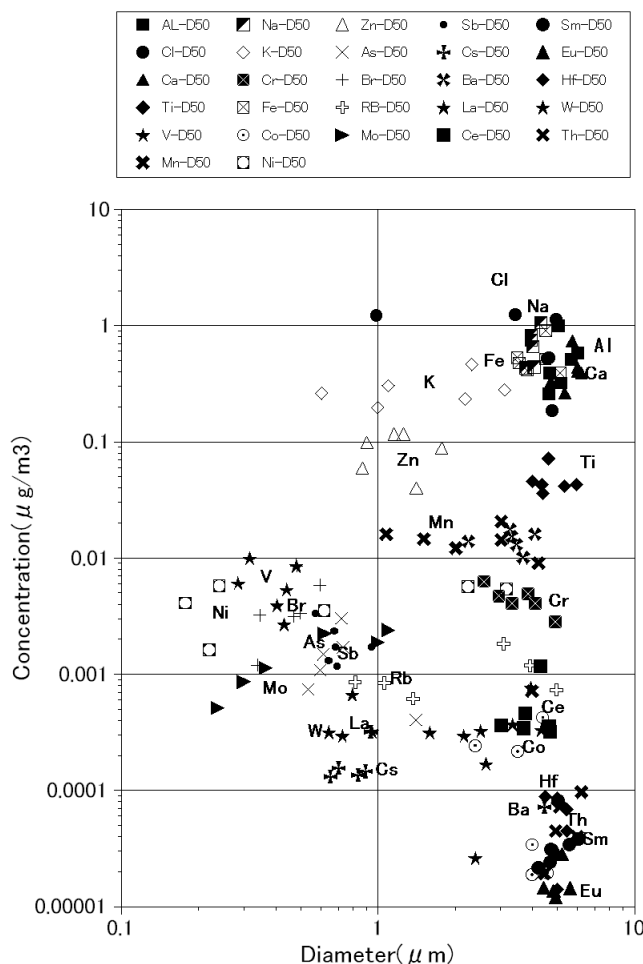


Fig.2 Scatter graph of d50 and total concentrations for each elements in the aerosols collected 2012 at Sakai.

K. Ninagawa, H. Nishido and S. Hamada

Okayama University of Science

### LOW TEMPERATURE TL OF ORDINARY

**CHONDRITES:** Induced TL (thermoluminescence), the response of a luminescent phosphor to a laboratory dose of radiation, reflects the mineralogy and structure of the phosphor, and provides valuable information on the metamorphic and thermal history of meteorites. Thermal metamorphism causes the production of feldspar, the major TL phosphor in ordinary chondrites, by the devitrification of feldspathic mesostasis. Primitive chondrites of petrologic subtype  $\leq 3.4$  with coefficient of variations ( $\sigma$  as a percentage of the mean) over 50%, of fayalite in the olivine have low TL sensitivities under 0.1. The sensitivity of the induced TL is usually used to determine petrologic subtype of unequilibrated ordinary chondrites [1]. On the other hand, TL sensitivity decreases 10-fold after shock-loading to 25-32 GPa [2], and terrestrial weathering makes TL sensitivity decrease 16-fold at maximum in Antarctic chondrites [3]. Then some secondary altered chondrites were reported to have low TL sensitivities, equivalent to primitive chondrites [4].

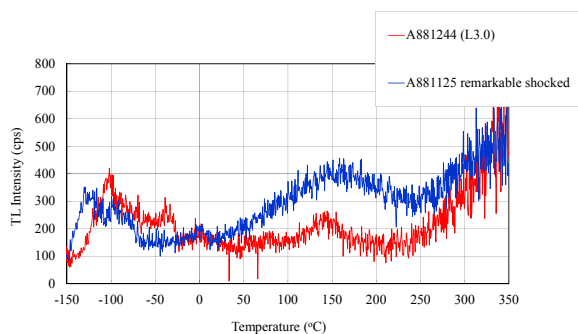


Fig.1. TL glow curves of a primitive ordinary chondrite of A881244 (L3.0) and remarkable shocked chondrite of A8811255.

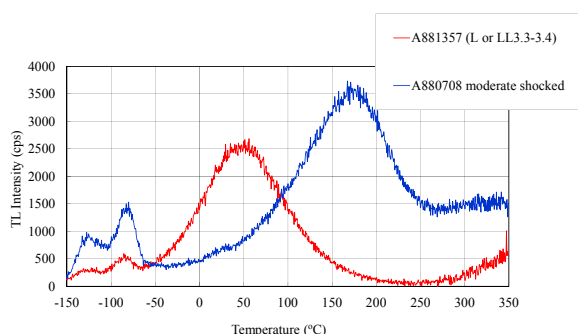


Fig.2. TL glow curves of A881357 and moderate shocked chondrite of A880708. The different peaks at 50 and 150 °C reflected to disordering of feldspar.

The induced TL of unequilibrated ordinary chondrites has been usually measured above room temperature. Then this time low temperature TL (-150~ 0 °C) were investigated to distinguish TL properties between primitive chondrites and secondary altered chondrites. TL glow curves of a primitive ordinary chondrite of A881244 (L3.0) and remarkable shocked chondrite of A8811255 is shown in Fig.1. TL glow curves of a primitive ordinary chondrite of A881357 (L or LL 3.3-3.4) and a moderate shocked chondrite of A880708. There are two peaks near -120 and -80°C lower than room temperature. However we could not find clear difference in TL properties between primitive chondrites and secondary altered chondrites.

**LOW TEMPERATURE TL OF UREILITE:** The ureilites are a major group of primitive achondrites. They are high fractionated rocks from an achondrite parent body. Ureilites are olivine-pyroxene rocks with interstitial C (graphite and microdiamonds) mixed with metal, sulfides, and minor silicate. Most ureilites are essentially devoid of feldspar [6]. This time we measured induced TL of five ureilites to check TL properties of ureilites. Fig.3 shows TL glow curve of Dar al Gani 319 and NWA3223. There were two large peaks at -100 and 0°C.

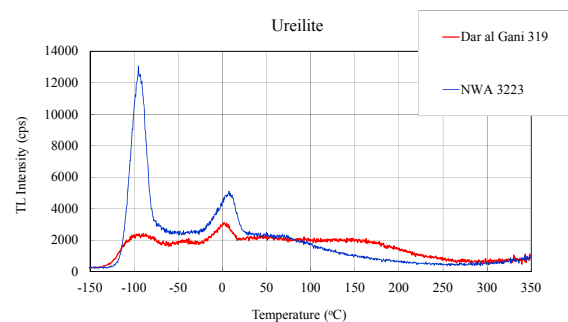


Fig.3. TL glow curve of ureilites, Dar al Gani 319 and NWA3223.

### REFERENCES:

- [1] Sears *et al.*, Proceedings of Lunar and Planetary Science **21** (1991) 493-512.
- [2] Hartmetz *et al.*, Proc. 17th Lunar Planet. Sci. Conf. (J. Geophysical Research), **91**, (1986) E263-E274.
- [3] Benoit and Sears, J. Geophys. Res., **104**, (1999) 14159-14168.
- [4] K. Ninagawa *et al.*, Antarctic Meteorite Research, **15** (2002) 114-121.
- [5] K. Ninagawa *et al.*, Antarctic Meteorite Research **18** (2005) 1-16.
- [6] Weisberg *et al.* Meteorites and the early solar System II, The University of Arizona Press, (2006) 19-52.

T. Yamagata, K. Shozugawa, R. Okumura<sup>1</sup>, K. Takamiya<sup>1</sup> and M. Matsuo

*Graduate School of Arts and Sciences, The Univ. of Tokyo*  
*<sup>1</sup>Research Reactor Institute, Kyoto University*

**INTRODUCTION:** Hypoxia is water mass with little dissolved oxygen (DO) [1]. In Tokyo Bay there are many large and deep dredged trenches, especially off the coast of Makuhari, Chiba. In dredged trenches severe hypoxia has been observed in summer, but the influence of dredged trenches on hypoxia is not revealed yet. Therefore, it is important to estimate the positional and seasonal variations of hypoxia by analyzing sediments.

To estimate the sedimentary environment related to redox conditions, various elements have been used. For example, Fe and Mn are used because their various chemical states on Eh-pH diagrams have become clear [2]. And U is used for the evaluation of weak reductive conditions because the redox potential of U(VI)/U(IV) is between Mn(IV)/Mn(II) and S(VI)/S(-II) [3]. We have applied the elements to evaluate the sedimentary environment in dredged trenches, which are under specific condition. In this study, sediment cores were collected from the Makuhari dredged trenches and concentrations of Fe, Mn, U, Th, and Ce in sediments were analyzed by instrumental neutron activation analysis (INAA).

**EXPERIMENTS:** The sediment samples were collected at a dredged trench (water depth 17.2 m) and reference site (non-dredged seabed, water depth 9.5 m) off the coast of Makuhari in Tokyo Bay in August 2013. Sediments were collected by a core sampler and water quality data were also obtained.

All cores were cut in the vertical direction at 0.6-3.0 cm intervals in the laboratory, and the samples were desalted and freeze-dried within a week.

Approximately 30 mg of sediments were packed in double polyethylene film bags to perform INAA. All samples were irradiated with neutrons at the pneumatic tube, Kyoto University Research Reactor. Three types of gamma-ray measurement were carried out corresponding to half-lives of elements. For analysis of Mn, samples were irradiated for 10 seconds at 1 MW, and then gamma-ray was measured for 600 seconds by Ge detector after 600 seconds cooling. Regarding U, samples were irradiated for 20 minutes at 1 MW or 4 minutes at 5 MW, and then gamma-ray was measured for 1200 seconds by Ge detector after 3-5 days cooling. Regarding Th and Ce, samples were irradiated for 20 minutes at 1 MW or 4 minutes at 5 MW, and the measuring time of gamma-ray was for 9000 seconds after 2-4 weeks cooling.

**RESULTS:** At the dredged trench surface water (< 9 m water depth) had DO about 6 mg/L, and bottom water (> 12 m water depth) had no DO. At both sites, concen-

trations of Fe and Mn in sediments were almost constant from the surface to the lower layers. It is well-known fact that the concentrations of Fe and Mn in sediments decrease due to eluviations of Fe<sup>2+</sup> and Mn<sup>2+</sup> when condition of seawater is reductive like hypoxia. The results indicate that the redox conditions of the surface of sediments were not so reductive as those in August 2011 [4].

On the other hand, we calculated Th/U and Ce/U ratios likewise Honda et al [5], and the depth profiles of the ratios in sediment are shown in Figure. The Th/U and Ce/U ratios in the upper layers (7-8 cm from the surface) were comparatively high, and the ratios settled down to almost constant lower values below 8 cm in depth at most sites. It is known that the concentrations of Th and Ce in sediments increase when condition of seawater is oxidative, and the concentration of U increases when condition of seawater is reductive. It is considered that the sedimentary environment of the upper layers is more oxidative than that of the lower layers. And focusing on the redox potential around U(VI)/U(IV), the method using Th/U and Ce/U ratios is well reflecting the redox states, because those of U, Th, Ce are thought to be preserved from the time of sedimentation.

As mentioned above, the method measuring the concentrations of various elements by INAA and focusing on different redox potentials of the elements is very useful to evaluate the sedimentary environment related to redox conditions.

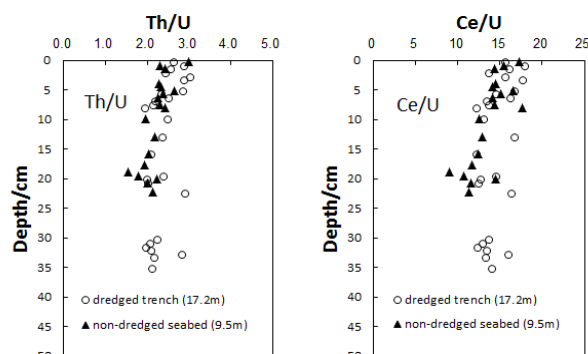


Figure. Depth profiles of Th/U (left) and Ce/U (right) ratios in the sediments collected from Tokyo Bay in August 2013.

### REFERENCES:

- [1] R.J. Diaz *et al.*, *Science*, **321** (2008), 926-929.
- [2] D.G. Brookins, in *Eh-ph diagrams for geochemistry* (Springer-Verlag, 1988).
- [3] D.R. Turner *et al.*, *Geochim. Cosmochim. Acta*, **45** (1981), 855-881.
- [4] T. Yamagata *et al.*, *J. Radioanal. Nucl. Chem.*, **303** (2015), 1179.
- [5] T. Honda *et al.*, *Bull. Soc. Sea Water Sci., Japan*, **57** (2003), 166-180 (in Japanese).

## CO5-4 Characteristics of Synthetic Calcite Thermoluminescence Studied for Paleoenvironmental Reconstruction of East Asia

N. Hasebe, K. Ito, K., K. Miura<sup>1</sup> and M. Ogata<sup>1</sup>

*Institute of Nature and Environmental Technology, Kanazawa University*

<sup>1</sup>*Graduate School of Natural Science and Technology, Kanazawa University*

**INTRODUCTION:** Luminescence dating observes the natural accumulated radiation damage caused by radioisotopes such as U and Th as the form of glow after stimulation by heating or lightening. Thermally stimulated luminescence from calcite shows strong red emission [1]. However, thermoluminescence dating of calcite is less popular because of some unknown problems; e.g., sensitivity change of calcite occurred through repeated heating of samples, possible anomalous fading, difference in characteristics of luminescence response against different kinds of radiation (e.g., gamma-ray, beta-ray, alpha-ray, and X-ray). When thermoluminescence characteristics of calcites are examined using natural occurring calcite, their response to the various radiations depends on minor chemistry (Fe, Mg, Mn and Sr). In this study, calcites with controlled impurity concentrations were synthesized and analyzed to evaluate relationship between multiple impurity concentration and thermoluminescence properties quantitatively.

**EXPERIMENTS:** Calcite were synthesized from sodium carbonate (>99.8wt%) and calcium chloride (>95 wt%). Iron (II) chloride (>99.0-102.0 wt%), magnesium chloride (>98.0wt%), and manganese chloride (>99.0-wt%) were added at different levels to produce calcites with different amount of impurity. Chemical composition of resultant calcite were measured by LA-ICP-MS. Gamma irradiation was carried out at the <sup>60</sup>Co gamma irradiation facility at Kyoto University Research Reactor. Then luminescence images were captured by the digital camera (Inagaki et al., 2010) and luminescence color and intensity were analyzed (Ogata et al., 2014).

**RESULTS:** Except for added elements, all of synthetic calcite contain ~30 ppm of strontium and ~6 ppm of barium. These elements must be contained in original reagent calcium chloride. Mn-added calcites include molybdenum which amount is proportional to the amount of added Mn. Mo must be contaminated to the reagent manganese chloride. As shown in Fig. 1, measured amount of impurity is proportional to the amount of added impurity. When thermoluminescence color image (TLCI) was captured, Mn added samples emitted strong red luminescence (Table 1). A sample with high impurity emit no luminescence. There may be some criteria in Mn concen-

tration to emit luminescence. The TLCI with small amount of Fe show colored pixels. However, these pixels may be noises because they are found in all color zones. Mg added samples emitted no luminescence. Therefore, Mg would not play significant role in luminescence characteristics.

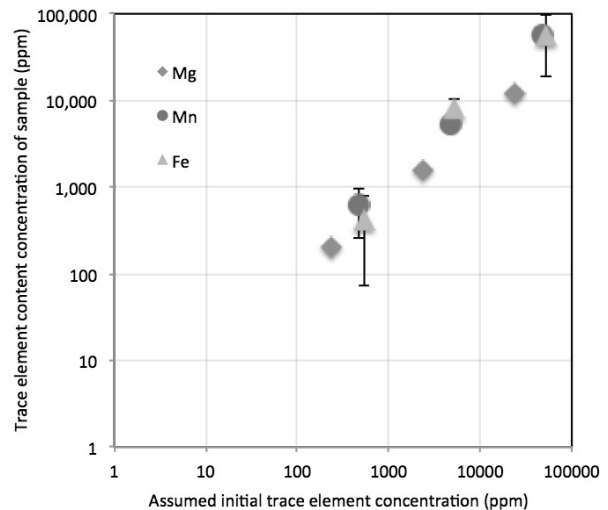


Fig. 1. The amount of elements measured by LA-ICP-MS is proportional to the amount of added elements

	R	Y	G	B	gap	Total
Mn (470ppm)	24592	328099	0	0	0	352691
Mn (4700ppm)	347579	0	0	0	0	347579
Mn(47000ppm)	0	26	0	0	0	26
Mg (240ppm)	58	14	0	11	6	89
Mg (2400ppm)	2	0	0	0	0	2
Mg (24000ppm)	3	17	0	0	0	20
Fe (530ppm)	3942	1269	402	68	635	6316
Fe (5300ppm)	26	18	0	87	7	138
Fe (53000ppm)	45	33	5	0	12	95
Pure calcite	40	0	0	0	0	40

Table 1. The results of TLCI investigation. Number of pixels in each color zone is counted. R stands for red, Y for yellow, G for green, B for blue, and gap for other color.

### REFERENCES:

- [1] A. Inagaki et al., *J. Geol. Soc. Japan* 116 (2010) XIX-XX
- [2] M. Ogata, *Sci. Rep. Kanazawa Univ.* 58 (2014) 1-12

## CO5-5 Fission Track Ages of Sedimentary Rocks from Accretionary Belt in the Kii Peninsula

H. Ohira and A. Takasu

Department of Geoscience, Shimane University

**INTRODUCTION:** Fission track dating was applied for sedimentary rocks of Kii peninsula, Wakayama prefecture. The aim of this study is to estimate depositional periods and thermal histories of sedimentary rocks in relation with burial-uplift processes during accretion process. In recent study, the Cretaceous Shimanto Belt in this area is newly divided into several accretionary complexes showing zonal structure, Ryujin, Miyama, Yukawa and Hanazono complexes, from the south to north [1]. FT age variations across the Shimanto belt in the Kii region and relationship between FT ages and thermal and burial/uplift history has been precisely discussed mainly for areas of the north side including a part of Hanazono complex [2].

**EXPERIMENTS:** Samples collected from each units of the Shimanto belt were crashed and sieved and heavy minerals were concentrated by common method. Zircon and apatite were abundant in almost samples but less amounts in the Miyama complex. Zircons were mounted in PFA Teflon, and then polished to reveal entire internal surface. Samples were etched in a NaOH-KOH eutectic melt at 225°C [3] for 20-32 hours and were irradiated at pneumatic tube of graphite facility (Tc-pn) of Kyoto University Reactor (KUR). FT densities were measured using optical microscope at 1000× magnification with a dry objective 100×. FT ages were calculated by trackkey program [4].

**RESULTS:** Fission track grain ages show wide variations in each sample but the youngest modes in histograms show a systematical tendency from south to north, probably corresponding to depositional period and thermal histories during burial-uplift process of each geological unit. Ranges and modes in histograms for each complexes are as follows; Ryujin (53-92Ma; 60Ma), Miyama (57-197Ma; 68Ma), Yukawa (94-300Ma; 126Ma), and Hanazono (55-93; 68Ma). FT ages become old from southernmost Ryujin complex toward the northern Yukawa complex, but the Hanazono complex in northernmost district show young age again. The gap of age between the Yukawa and Hanazono complex and rejuvenation of FT age in the Hanazono complex is compatible

with that the “Yanase Fault” is important thrust system which dividing complexes of this area and the Hanazono complex was exposed to relatively higher temperature due to deep burial. Almost FT grain ages from the Yukawa complex show entirely older than the estimated depositional period, indicating that sample was not affected by heating up to enough temperature to reset FT ages. On the contrary, the youngest age component in the Ryujin complex (59Ma) is significantly younger than the limit of depositional period (68-78Ma). This result probably indicates that most of FT grain ages of Ryujin complex were reset by thermal affect during burial process to a deeper level, or the depositional age of the Ryujin complex is actually younger than previous interpretation. Detail track length measurement will be required for the solution of above discussion.

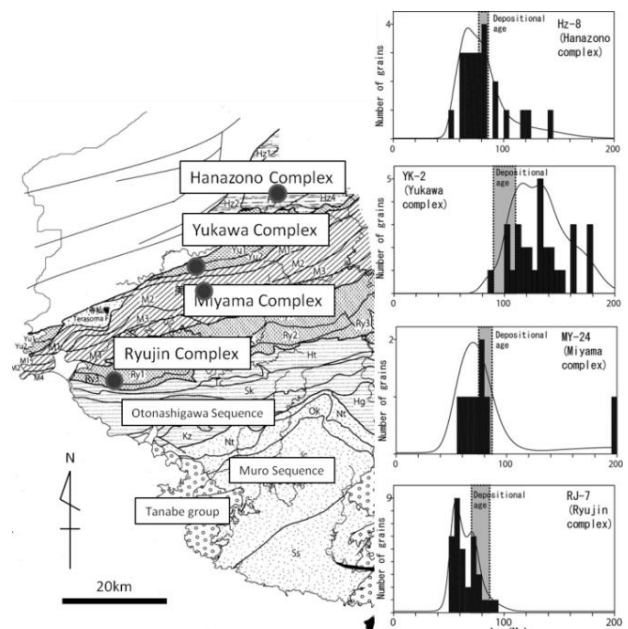


Fig.1 FT age histogram and geological map with each complex boundary [5].

- [1] Suzuki H. and Nakaya S., 2012, The Assoc. Geological Collaboration in Japan, Monograph 59, 273-282 (in Japanese with English abstract).
- [2] Hasebe N. and Tagami T., 2001, Tectonophysics 331, 247-267.
- [3] Gleadow A.J.W. *et al.*, 1976, Earth and Planetary Science Letter, 33, 273-276.
- [4] Dunkle, I., 2002, Computer & Geosciences, 28, 3-12.
- [5] Suzuki H., 2012, The Assoc. Geological Collaboration in Japan, Monograph 59, 101-110 (in Japanese with English abstract)

## CO5-6 Trace Amounts of Halogens (Cl, Br and I) in Manganese Nodule Reference Materials

M. Ebihara and S. Sekimoto<sup>1</sup>

Graduate School of Science, Tokyo Metropolitan University

<sup>1</sup>Research Reactor Institute, Kyoto University

**INTRODUCTION:** Accurate and reliable data of halogen abundance have been rarely reported for terrestrial samples, such as manganese nodule materials. Since halogens differ in volatility from element to element, their content and relative abundance are highly informative when discussing the petrogenesis of such samples. Recently, we have improved the radiochemical neutron activation analysis (RNAA) procedure for trace amounts of halogens (Cl, Br and I) [1]. In this study, our RNAA was applied to two manganese nodule materials that are available in U.S. Geological Survey (USGS) and then, our RNAA values were compared with the literature values.

**EXPERIMENTS:** Trace amounts of Cl, Br and I in the two manganese nodules (Nod-P-1 and Nod-A-1) were determined by RNAA. The RNAA procedure is described elsewhere [1-2]. Those samples were repeatedly analyzed more than two times.

**RESULTS:** The two manganese nodules (Nod-P-1 and Nod-A-1) analyzed using RNAA in this study were also analyzed using inductively coupled plasma double focusing sector field mass spectrometry (ICP-SFMS) [3] for bromine and iodine. Our RNAA values and the ICP-SFMS values are shown in Table 1. Before analysis by ICP-SFMS, the nodule materials were subjected to the acid digestion procedure, in which the nodule materials are heated with the mixture of concentrated nitric, hydrochloric and hydrofluoric acids by using microwave. The digestion solution was diluted appropriately and then introduced into the ICP-SFMS instrument.

**Table 1:** Cl, Br and I contents in USGS manganese nodule materials analyzed by RNAA in this study<sup>a</sup> and from the Literature

sample		Cl(mg kg <sup>-1</sup> )	Br(mg kg <sup>-1</sup> )	I(mg kg <sup>-1</sup> )
Nod-P-1	RNAA (n = 4)	1380 ± 140	5.93 ± 0.76	157 ± 17
	ICP-SFMS <sup>15</sup>	- <sup>b</sup>	30.3 ± 2.2	31.4 ± 0.3
Nod-A-1	RNAA (n = 2)	4410 ± 160	14.8 ± 0.5	367 ± 9
	ICP-SFMS <sup>15</sup>	- <sup>b</sup>	40.9 ± 0.7	47.7 ± 3.2

<sup>a</sup>Mean values followed by standard deviations (1σ) (n=3, 4). Mean values followed by an uncertainty which is simply the value calculated from two individual uncertainty values. (n=2) <sup>b</sup>Not reported.

Our RNAA data for Nod-P-1 and Nod-A-1 are not consistent with the literature data obtained by ICP-SFMS for both bromine and iodine. As for iodine the ICP-SFMS values are lower than the RNAA values. Such an inconsistency between RNAA values and ICP-SFMS values also may be derived from the loss of iodine in the acid digestion procedure with heating by the microwave. To prevent the loss of iodine, the digestion solution should not be heated in principle, or heating of the digestion solution must be achieved with extreme care. Regarding bromine, on the other hand, the ICP-SFMS values are higher than the RNAA values by a factor of about three to five. Such an inconsistency between RNAA values and ICP-SFMS values may be due to the ability of this ICP-SFMS instrument, especially to background [4]. Bromine is determined by ICP-SFMS and/or ICPMS using the isotope <sup>79</sup>Br and <sup>81</sup>Br. The mass of those two bromine isotopes is next and very close to the biatomic (<sup>40</sup>Ar<sup>40</sup>Ar)<sup>+</sup> molecule of mass 80. Since argon is so abundant in the plasma of the ICP-SFMS and/or ICPMS, the combination of two <sup>40</sup>Ar ions causes a large peak at mass 80 whose peak tail could interfere with either stable isotope of bromine. Additionally, there are several potential interferences on <sup>79</sup>Br and <sup>81</sup>Br; (<sup>40</sup>Ar<sup>39</sup>K)<sup>+</sup>, (<sup>63</sup>Cu<sup>16</sup>O)<sup>+</sup> and (<sup>40</sup>Ar<sup>38</sup>Ar<sup>1</sup>H)<sup>+</sup> interference with <sup>79</sup>Br and (<sup>40</sup>Ar<sup>41</sup>K)<sup>+</sup>, (<sup>65</sup>Cu<sup>16</sup>O)<sup>+</sup> interference with <sup>81</sup>Br signals, respectively [4]. To quantify <sup>79</sup>Br successfully without interference of (<sup>40</sup>Ar<sup>39</sup>K)<sup>+</sup> and (<sup>63</sup>Cu<sup>16</sup>O)<sup>+</sup> nor of (<sup>40</sup>Ar<sup>38</sup>Ar<sup>1</sup>H)<sup>+</sup>, the ICP-SFMS instrument should be operated in resolution (m/δm) of >10000 or >5000, respectively. (A required resolution for successful quantification of <sup>79</sup>Br is explained in the Supporting Information.) In case of the literature values for bromine, however, the ICP-SFMS instrument was operated in medium resolution mode (m/δm=4500) for <sup>79</sup>Br, and interference of (<sup>40</sup>Ar<sup>39</sup>K)<sup>+</sup> and (<sup>63</sup>Cu<sup>16</sup>O)<sup>+</sup> cannot be removed from <sup>79</sup>Br signal. A possible explanation of higher bromine values in ICP-SFMS than in RNAA could be an overestimation due to the interference at mass 79 in the ICP-SFMS instrument. Since the ICP-SFMS operation in high resolution mode (HRM) is generally the operation in resolution (m/δm) of 9000-10000, it is fundamentally impossible to quantify <sup>79</sup>Br successfully without interference of (<sup>40</sup>Ar<sup>39</sup>K)<sup>+</sup> and (<sup>63</sup>Cu<sup>16</sup>O)<sup>+</sup> even using the HRM. This suggests that bromine-separation as a pretreatment of samples is essential for bromine-determination using ICP-SFMS and/or ICPMS.

### REFERENCES:

- [1] S. Sekimoto and M. Ebihara, *Anal. Chem.*, **85** (2013) 63366341.
- [2] S. Sekimoto and M. Ebihara, in preparation.
- [3] M.D. Axelsson *et al.*, *Analyst*, **127** (2002) 76-82.
- [4] J. Hammerli *et al.*, *Chem. Geol.*, **337-338** (2013) 75-87.

## CO5-7 Application of Neutron Activation Analysis to Micro Gram Scale of Solid Samples

S. Sekimoto, N. Shirai<sup>1</sup>, M. Ebihara<sup>1</sup>

Research Reactor Institute, Kyoto University

<sup>1</sup> Graduate School of Science, Tokyo Metropolitan University

**INTRODUCTION:** Since instrumental neutron activation analysis (INAA) is a non-destructive and multi-elemental analysis method, it is suitable for precious samples and, especially, for such specimens as those highly desired to be neither physically decomposed nor chemically dissolved. Meteorites are the best example for such samples. Chondritic meteorites (chondrites) and iron meteorites contain relatively high contents of Co and Ir compared with those in the earth crust. As Co and Ir have high sensitivity in NAA, they can be good markers for the identification of such extraterrestrial materials. In NAA of chondrites, a few tens mg of specimen is commonly used. For such a case, a few hundred  $\mu\text{g kg}^{-1}$  of Ir and a few hundred  $\text{mg kg}^{-1}$  of Co can be reliably determined. When an extremely small size (e.g., micro gram) of samples such as micrometeorites recovered on the Earth surface and tiny particles returned from extraterrestrial asteroids are to be analyzed by INAA, the conventional INAA procedure used for a few tens mg is not suitable. For such tiny samples, neutron irradiation with high neutron flux and long irradiation time (namely, high neutron dose) is required. For the irradiation with high neutron dose, polyethylene bags for holding samples are not usable because they are prone to radiation damage. Polyethylene bags are also not suitable for holding tiny grain samples. It is, therefore, very important to design an appropriate sample holder for irradiating small grain samples. As we use a relative method for quantification, in this report, the preparation of reference samples and the evaluation for their suitability are described in detail.

**EXPERIMENTS:** Two reference samples with different elemental compositions were used; the Allende meteorite powder (1.66 mg) prepared by the Smithsonian Institution (USMN 3529; split 22 and position 6) and the basaltic rock reference sample JB-1 prepared by Geological Survey of Japan (1.12 mg). Each sample was sealed into a synthesized quartz tube (1 mm inner  $\phi$  and 2.7 mm outer  $\phi$  x 35 mm length), which was then wrapped with Al foil for the safety. The neutron irradiation was performed for 45 hours at the hydro-irradiation port of Kyoto University Reactor (KUR) in Kyoto University Research Reactor Institute (KURRI) under 1MW operation.

**RESULTS:** For quantification in INAA, two reference samples (the Allende meteorite and the JB-1 basalt) having different elemental contents were used. We have conducted similar INAA experiments where tiny grain samples collected by the spacecraft were analyzed by

using Allende and JB-1 as reference samples. Hereafter, these experimental runs named run-2 [1] and run-3 [2] are discussed in comparison with the present study, which is named run-1. It is meaningful to compare the activity of radioactive nuclides used in INAA for two different reference samples. We discuss the gamma rays counting rate per unit mass for each target element, hereafter gamma-ray intensity, among three runs. The gamma rays counting rate is gamma ray counts per second and correspond to gamma ray energies designated for individual nuclides ( $^{24}\text{Na}$ ,  $^{46}\text{Sc}$ ,  $^{59}\text{Fe}$ ,  $^{140}\text{La}$ ,  $^{153}\text{Sm}$ ,  $^{58}\text{Co}$ ,  $^{60}\text{Co}$ ,  $^{65}\text{Zn}$  and  $^{51}\text{Cr}$ ). Those nine nuclides were determined both for Allende and JB-1. Relative gamma-ray intensities of  $^{24}\text{Na}$ ,  $^{46}\text{Sc}$  and  $^{59}\text{Fe}$  in both reference samples are highly consistent for the three runs. Such a consistency can also be seen for Fe reagents. Kong and Ebihara [3] evaluated the consistency in elemental contents in the mg size of JB-1 and confirmed that JB-1 is well homogenized for its use in mg. We confirm that Allende can also be used as a reference sample for mg scale of sample at least for Na, Sc and Fe. On the other hand, Allende and JB-1 show a small inconsistency, most of which may be due to poor counting statistics for either sample. For example, Allende tends to have relatively low contents of rare earth elements (La and Sm), whereas JB-1 has a low content of Ni and Zn. Depending upon elemental contents, either Allende or JB-1 may be used for a reference sample.

There appears an apparent inconsistency in Cr data between the two reference samples, with JB-1 having systematically higher gamma-ray intensity. This is undoubtedly due to an erroneous reference value ( $425 \text{ mg kg}^{-1}$ ) of Cr for JB-1. If a proposed value ( $475 \text{ mg kg}^{-1}$ ) [3] is instead used, an excellent consistency can be seen as shown in Fig. 1 for  $^{51}\text{Cr}$ .

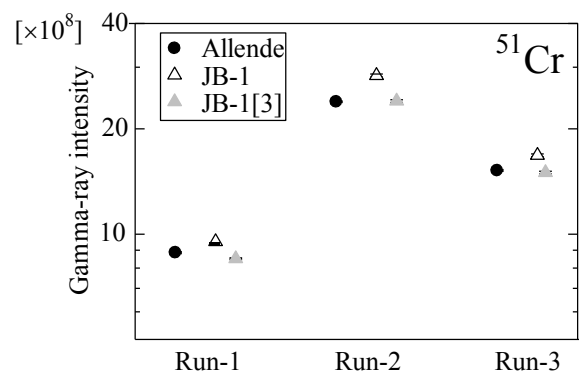


Fig. 1. Gamma-ray intensities of  $^{51}\text{Cr}$  in reference monitors for run-1, run-2 and run-3.

### REFERENCES:

- [1] M. Ebihara *et al.*, Meteorit. Planet. Sci., **50** (2015) 243-254.
- [2] M. Ebihara *et al.*, Science, **333** (2011) 1119-1121.
- [3] P. Kong and M. Ebihara, Geochem. J., **31** (1997) 339-344.

## CO5-8 Probability distribution of SEL occurred on on-board computer (OBC) mounted on small-scale satellite

H. Masui, T. Tomioka, K. Taniwak, M. Cho and K. Takamiya<sup>1</sup>

Kyushu Institute of Technology

<sup>1</sup>Research Reactor Institute, Kyoto University

**INTRODUCTION:** Recently universities and venture businesses actively develop small-scale satellites. For the small-scale satellites, many COTS (Commercial-off-the-shelf) components are used. The COTS components are not enough durable for space radiation environment. In particular, a microprocessor embedded to OBC suffers a problem of Single Event Latch-up (SEL). Horyu-2 was the small-scale satellite developed by Kyushu Institute of Technology (KIT) and actually suffered many on orbit anomalies due to SEL[1-2]. Therefore, the radiation test is important for small-scale satellite using the COTS to characterize the radiation effect and to find most durable COTS. However, a radiation test using an accelerator is not readily available. Since 2012, KIT has been conducting radiation test using <sup>252</sup>Cf for small-scale satellite. In this report, recent radiation tests, using <sup>252</sup>Cf, has been reported. This ground experiment data was analyzed and compared with the on-orbit data acquired from Horyu-2 in order to investigate the nature of anomaly.

**EXPERIMENTS:** Figure 1 shows the schematic of test configuration. A microprocessor, as device under test (DUT), was set in a vacuum chamber. The pressure during the test was approximately 30 Pa. The model number of microprocessor was HD64F36057FZJV and its plastic cover was removed. The same model microprocessor was mounted on Horyu-2. The radiation source of <sup>252</sup>Cf was mounted on XYZ stage. By changing a distance from the test sample to <sup>252</sup>Cf, radiation flux was calculated and controlled. DAQ and PC1 measured a voltage and current of the microprocessor. PC2 monitored the operation of microprocessor with RS232 communication. Just after the SEL occurred each time, a reset command was sent to the microprocessor. If the microprocessor was not recovered due to SEL, power was turned off.

**RESULTS:** 100 times SELs were observed and the time between SELs was measured for each flux condition. Figure 2 shows the probability distribution of a SEL occurrence with respect to time[3] at three different distances. As shown in Fig. 2, the time between SLEs is increased with increasing of the flux and the probability follows the Poisson distribution. Table 1 shows a SEL occurrence time and the cross-section for ground experimental. On-orbit data from 2012 to 2015 is also shown. A simple average SEL occurrence time was  $1.2 \times 10^7$  sec (= 139 days) from the orbit data. The cross-section derived

from the ground test is  $2.8 \times 10^5$  to  $1.4 \times 10^6$  times the cross-section derived from the on-orbit data.

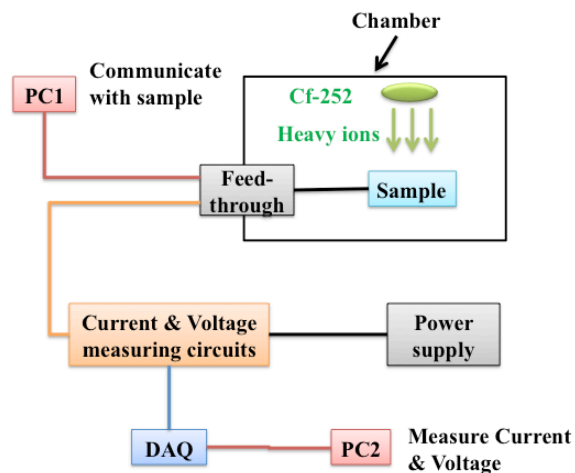


Fig. 1 Test configuration

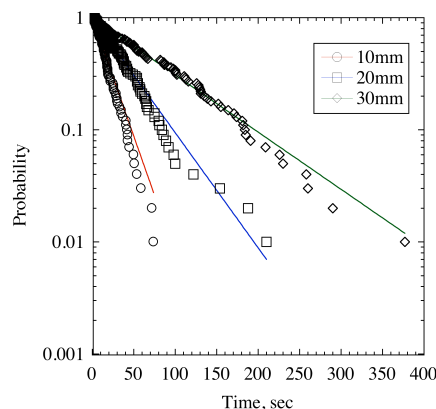


Fig. 2 Probability of SEL occurrence for various fluxes

Table 1 Comparison between <sup>252</sup>Cf test and on-orbit anomaly

	<sup>252</sup> Cf test			Orbit
	37	13	6.4	
Flux, 1/cm <sup>2</sup> /s	37	13	6.4	64
Simple average time, s	19.3	42.2	86.3	$3.4 \times 10^6$
Cross section of SEL, x 10 <sup>-3</sup> cm <sup>2</sup>	1.3	1.8	1.8	$1.3 \times 10^{-6}$

### REFERENCES:

- [1] M. Cho et al., The Japan Society for Aeronautical and Space Sciences, 12(0), 17-24, 2013.
- [2] Y. Seri et al., SSC13-X-8, Small Satellite Conference, August, 2013.
- [3] T. Tomioka et al., Acta Astronautica, submitted for publication.

採択課題番号 26053

カリフォルニウム線源を使用した衛星搭載用

通常採択

オンボードコンピュータに発生するシングルイベントの模擬試験および試験方法の確立

(九工大・先端) 増井博一、富岡孝裕、谷脇康洋、趙孟佑 (京大・原子炉) 高宮幸一

## CO5-9 Instrumental Photon Activation Analysis of Geological and Cosmochemical Samples

N. Shirai, S. Sekimoto<sup>1</sup>, M. Ebihara

Department of Chemistry, Tokyo Metropolitan University  
<sup>1</sup>Research Reactor Institute, Kyoto University

**INTRODUCTION:** Bulk chemical compositions for terrestrial and cosmochemical materials are significantly important to elucidate the formation, evolution processes and magmatism of planetary bodies. Compared to geological samples, cosmochemical samples pose several severe requirements to their analytical methods for chemical compositions. High sensitivity and accuracy for as many as elements as possible are required for analytical methods applied to such samples because of the limitation of sample amounts usable for analysis. Non-destructive analysis for many elements is equally favorable. Nuclear analytical methods represented by prompt gamma-ray analysis (PGA), instrumental neutron activation analysis (INAA) and instrumental photon activation analysis (IPAA) meet almost all these requirements. Among these nuclear analytical methods, INAA has been commonly used as an analytical tool in cosmochemistry for a long time, while PGA and IPAA have not been very often applied to cosmochemical samples.

In IPAA,  $(\gamma, n)$  reaction is used for the determination of elemental abundances which is an opposite reaction used in INAA. Thus, IPAA could determine elemental abundances which cannot or hardly be determined by INAA. Usually samples are irradiated by using 30 MeV electrons in IPAA. However, corrections of interferences caused by secondary nuclear reactions such  $(\gamma, p)$  and  $(\gamma, pn)$  are necessary. Although the sensitivity obtained by activation with 20 MeV electrons are suppressed compared with the activation with 30 MeV electrons, activation with 20 MeV electron reduces the degree of such interference reactions. In this study, we performed IPAA by using a linear electron accelerator at Kyoto University Research Reactor Institute (KURRI) and compared the results obtained by the activation with 20 MeV with those with 30 MeV.

**EXPERIMENTS:** Three GSI standards materials namely JA-2 (andesite), JB-3 (basalt) and JR-1 (rhyolite) and one cosmochemical sample (Allende meteorite) were analyzed by IPAA. Chemical reagent sample, Fe<sub>2</sub>O<sub>3</sub> powder and Cr, Mn and Ni metals were also irradiated to correct the interference reactions. Samples and chemical reagents were taken into a sample container (9 mm $\phi$ ) made of highly Al foil. Five to ten samples were stacked, among which thin foil disk (9 mm $\phi$ ) of Au as a monitor of the intensity of photon are placed. Samples in a block were put in a quartz tube. We used a linear electron ac-

celerator at the Research Reactor Institute, Kyoto University. Electrons were accelerated by the linear accelerator to about 30 and 20 MeV. After irradiation (about 30 hours), samples were taken into new Al foil and measured at the Laboratory of Radioisotopes, Tokyo Metropolitan University. For comparative method, JB-1 was used as reference standard.

**RESULTS:** Table 1 shows the interfering reactions and their contributions to nuclides produced by corresponding reactions for activation with 20 MeV and 30 MeV electrons. As shown in Table 1, significant contributions from interfering reactions were found in activation with 30 MeV electrons. Thus, determinations of Cr, Co and Mn abundances need the correction of corresponding interferences. As expected, contributions from interfering reactions with 20 MeV electrons were lower than those in activation with 30 MeV electrons.

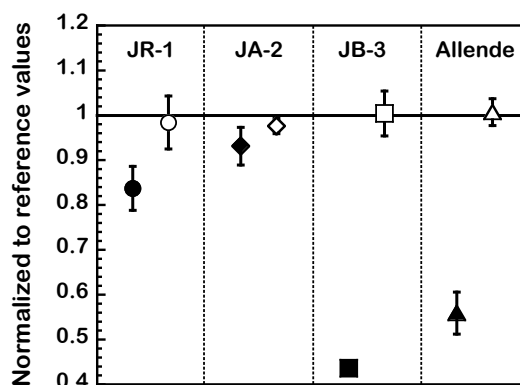


Figure 1. Our Mn values obtained by using 20 and 30 MeV electrons are compared with the corresponding reference values. Solid and open symbols represent that data are determined by using 30 and 20 MeV electrons, respectively.

A total of 17 elements (Ca, Sc, Ti, Cr, Mn, Fe, Co, Ni, Zn, As, Rb, Y, Zr, Nb, Cs, Ba and Ce) were determined in geological reference materials and the Allende meteorite. Our Cr and Mn values obtained from activation with 30 MeV electrons were different from literature values. Our Mn values obtained by using 20 and 30 MeV electrons are compared with reference values in Figure 1. For four samples, Mn values obtained by using 20 MeV electrons are consistent with reference values, while those by using 30 MeV electron are lower than literature values. Differences of Mn values in JB-3 and Allende between 30 and 20 MeV electrons are more remarkable than those in JR-1 and JA-2. Fe/Mn ratios of JR-1, JA-2, JB-3 and Allende are 8.1, 52, 60 and 162, respectively. In consideration of Fe/Mn ratios, overcorrections of the interfering reactions were responsible for these differences. For other elements, there were no differences between the two sets of our values obtained from the activations with 20 and 30 MeV electrons, which were consistent with literature values.

Table 1. Interfering reaction and correction rate for interference.

Reaction used for determination	Interfering reaction	Correction rate	
		30 MeV	20 MeV
<sup>52</sup> Cr( $\gamma, n$ ) <sup>51</sup> Cr	<sup>56</sup> Fe( $\gamma, \alpha n$ ) <sup>51</sup> Cr	0.036 mgCr/gFe	-
<sup>59</sup> Co( $\gamma, n$ ) <sup>58</sup> Co	<sup>60</sup> Ni( $\gamma, pn$ ) <sup>58</sup> Co	3.7 mgCo/gNi	0.88 mgCo/gNi
<sup>55</sup> Mn( $\gamma, n$ ) <sup>54</sup> Mn	<sup>56</sup> Fe( $\gamma, pn$ ) <sup>54</sup> Mn	6.2 mgMn/gFe	0.1 mgMn/gFe

採択課題番号 26067 放射化分析による宇宙・地球化学的試料の元素組成の定量 通常採択  
 (首都大学東京理工) 白井直樹、海老原充 (京大・原子炉) 関本俊

A. Hashiguchi, M. Yoneda, Y. Fujikawa<sup>1</sup>

Graduate School of Engineering, Kyoto University

<sup>1</sup>Research Reactor Institute, Kyoto University

**INTRODUCTION:** Perfluoro compounds (PFCs), characterized by high chemical and thermal stability, have been widely used in the world as water and oil repellent, car wax and fire extinguisher, etc. Among various PFCs, perfluorooctane sulfonate (PFOS), a linear perfluoroalkyl sulfonate with eight carbon-chain length, has been noted for its high bioaccumulation potential to wildlife and persistence in the environment. Among the various environmental problems associated with this recalcitrant substance, we were most interested in development of a practical technology that could be used to polish-up the wastewater containing PFOS.

Existing practical treatment methods for removal of PFOS from sewage effluent or wastewater are membrane filtration (especially reverse osmosis), or adsorption using activated carbon. Use of these methods has a figure of merit as they are already installed in many treatment plants, and the operation and management protocols for various micro-pollutants are fairly well established. On the other hand, PFOS is not decomposed by these methods, only concentrated in the reject or adsorbents. A technique that can decompose PFOS in the concentrate is needed.

Photo-assisted methods have been known to be effective for decomposition of pollutants in air and water. The treatment is done either via direct photoexcitation of the pollutant or mediated processes involving highly reactive radicals generated by photolysis. UV light is commonly used for the technology, but for particularly recalcitrant pollutants such as PCBs and chloro-fluoro aliphatic carbons,  $\gamma$  ray irradiation has been proved to be most effective. The OH radical, solvated electron, and radical or cation of isopropyl alcohol (added as a source of organic radicals), produced in the medium by  $\gamma$  ray, degraded the pollutants through reductive dehalogenation processes.

In our study, we irradiated the PFOS in various media with  $\gamma$  ray to investigate the possibility of decomposition of PFOS via direct photolysis or radical reactions.

**EXPERIMENTS:** A 414 TBq (as of February, 2008) <sup>60</sup>Co in  $\gamma$  ray irradiation facility in KURRI was used as a  $\gamma$  ray source. All the reagents used were Japan Industrial Standard reagent grade unless stated otherwise. Known amount of PFOS powder purchased from Wako Chemical Industry was dissolved in methanol (HPLC grade), and was used to spike alkaline isopro-

pyl alcohol (IPA) and alkaline potassium persulfate solutions. Both solutions were purged with nitrogen gas before the irradiation. The use of persulfate was tested because the substance is a known radical initiator that produces sulfate radical through  $S_2O_8^{2-} \rightarrow 2SO_4^{\cdot -}$  reaction. As a control, ethanol (a radical scavenger) spiked with PFOS was also irradiated. The IPA and persulfate solution was subjected to solid phase extraction by Oasis HLB (strongly hydrophilic and lyophobic, Waters) resin prior to determination of PFOS. Direct photolysis of solid PFOS by gamma-ray was investigated by irradiation of a 20 $\mu$ L drop of PFOS (concentration: 1g/L-methanol), dried on a microscope slide, and covered with a cover glass.

Irradiation dose was estimated by ceric sulfate dosimeter utilizing the reduction of  $Ce^{4+}$  to  $Ce^{3+}$  by the radiation, or the calculation considering the distance and angle from the <sup>60</sup>Co radiation source. Concentrations of PFOS in sub-samples collected before and after the irradiation were determined by UPLC-MS/MS (Waters).

**RESULTS:** Fig.1 shows the decrease in the numbers of PFOS molecules after gamma-ray irradiation of the dried residue of PFOS solution. The decrease of PFOS molecules was roughly proportional to the adsorbed dose. Interestingly, the rate of decrease was strongly dependent

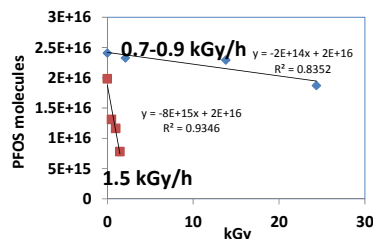


Fig. 1 Decomposition of dried PFOS residue with time (kGy)

on the dose rate, and was faster at the higher dose rate. Since the generation of radicals in the dried residue is negligible, the decomposition of PFOS is attributed to photoexcitation of PFOS followed by its decomposition. It has been known that upon irradiation with UV, perfluorooctanoic acid (PFOA), one of the PFCs known for its refractoriness, was decomposed, and the mechanism of decomposition was ascribed to direct photolysis rather than to radical reaction [1]. On the other hand, the decomposition of PFOS by UV has not been found so far. The present result indicates that high energy photon (1.16 and 1.33 MeV  $\gamma$  ray from <sup>60</sup>Co in this case) was probably needed to induce the direct photolysis of PFOS.

The decomposition of PFOS in ethanol was 30% (initially  $2.3 \times 10^{15}$  molecules) after 42 kGy (dose rate 2.7 kGy/h) of irradiation. After 38 kGy (dose rate 0.67 kGy/h) of irradiation, only 6 % of PFOS was decomposed in alkaline persulfate, while in IPA, 85% of PFOS was decomposed, due probably to the radical reactions.

**REFERENCES:**

[1] R. R. Giri *et al.*, Water Sci. & Technol., 63 (2011) 276-282.